The Journal of Undergraduate Research in Physics

CONTENTS

VOLUME 3, NUMBER 1

SPRING, 1984

Published by Guilford College
for
The American Institute of Physics and The Society of Physics Students

THE JOURNAL OF UNDERGRADUATE RESEARCH IN PHYSICS

This journal is devoted to research work done by undergraduate students in physics and its related fields. It is to be a vehicle for the exchange of ideas and information by undergraduate students. Information for students wishing to submit manuscripts for possible inclusion in the Journal follows.

ELIGIBILITY

The author must have performed all work reported in the paper as an undergraduate. The subject matter of the paper is open to any area of pure or applied physics or physics related field.

SPONSORSHIP

Each paper must be sponsored by a full-time faculty member of the department in which the research was done. A letter from the sponsor to the editor must accompany the manuscript if it is to be considered for publication.

FORM

The manuscript should be typed, double spaced, on 8 1/2 x 11 inch sheets. Margins of about 1 1/2 inch should be left on the top, sides, and bottom of each page. Papers should be limited to twelve pages of text in addition to an abstract and appropriate drawings, pictures, and tables.

GENERAL STYLE

All papers must conform to the Style Manual of the American Institute of Physics. Each paper must be prefaced by an abstract that does not exceed 250 words.

ILLUSTRATIONS

Line drawings should be made with black India ink on plain white paper. If a graph is drawn on co-ordinate paper, the paper must be lined blue. Important lines should be ruled in black. Each figure or table must be on a separate sheet. Photographs must have a high gloss finish.

CAPTIONS

A brief caption should be provided for each illustration or table, but it should not be part of the figure. They should be listed together at the end of the manuscript.

EQUATIONS

Equations should appear on separate lines and may be written in black India ink.

FOOTNOTES

Footnotes should be typed double spaced and grouped together in sequence at the end of the manuscript.

SUBMISSION

Two copies of the manuscript should be sent to:

Dr. Rexford E. Adelberger, Editor
THE JOURNAL OF UNDERGRADUATE RESEARCH IN PHYSICS
Physics Department
Guilford College
Greensboro, NC 27410

SUBSCRIPTION INFORMATION

The Journal will be published biannually with issues appearing in April and October of each year. There will be two issues per volume.

TYPE OF SUBSCRIBER	PRICE PER VOLUME
Individual	$ 5.00
Institution	$10.00

Foreign subscribers add $2.00 for postage

To receive a subscription, send your name, address, and check made out to The Journal of Undergraduate Research in Physics (JURP) to:

Journal of Undergraduate Research in Physics
Physics Department
Guilford College
Greensboro, NC 27410

BACK ISSUES

Back issues may be purchased by sending $10.00 per volume to the editorial office.

ISSN 0731 - 3764

The Journal of Undergraduate Research in Physics is published by Guilford College for the American Insititute of Physics and the Society of Physics Students.

VOLUME 3 1984

The Journal of Undergraduate Research in Physics

Published by Guilford College
for
The American Institute of Physics and The Society of Physics Students

ISSN 0731 - 3764

STUDY OF CHARGE ASYMMETRY IN THE REACTION $e^+ + e^- \rightarrow \mu^+ + \mu^-$ WITH THE FORWARD COUNTERS OF THE MARK J DETECTOR AT PETRA

Tak Leuk Kwok
Physics Department
California Institute of Technology
Pasadena, CA 91125

ABSTRACT

The forward-backward charge asymmetry in the reaction $e^+ + e^- \rightarrow \mu^+ + \mu^-$ at E_{cm} (center-of-mass energy) = 34 GeV in the angular range $0.5 < |\cos\theta| < 0.8$ has been determined to be:

$$A_{\mu\mu} = (-16.3 \pm 3.7)\ \%$$

This is in agreement with the standard unified electroweak theoretical prediction of $(-14.2 \pm 1.8)\%$. An attempt was made to determine the asymmetry down to $|\cos\theta| < 0.9$, but a lack of bending power in the detector at the end of the muon acceptance resulted in insufficient momentum resolution to reliably determine the muon charge. Further analysis of the track fitting procedures in the region is needed.

INTRODUCTION

PETRA (Positron Elektron Tandem Ringbeschleuniger Anlage) is currently the world's highest energy e^+e^- colliding beam machine. At the present, it reaches a center-of-mass energy (E_{cm}) of 46 GeV. It has 4 experimental halls, one of which is called MARK J. Figure 1 shows a schematic layout of PETRA and the experiments.

The MARK J detector (located at one of the intersection point of the e^+ and e^-beams) is designed to distinguish charged hadrons, electrons, muons, neutral hadrons and photons produced by the collision of the two beams and to measure their directions and energies. A detailed description of the individual components of the detector can be found elsewhere (1). Having a close to uniform efficiency, almost 4π solid angle acceptance, the MARK J detector is capable of fulfilling a broad range of physics objectives, one of which is to measure the charge asymmetry in $e^+ + e^- \rightarrow \mu^+ + \mu^-$.

The observation of weak neutral currents (2) gave crucial support to the idea that a neutral massive gauge boson was one of the mediators of the weak interaction. One of the detectable effects of the neutral weak boson (Z^0) at PETRA is the forward-backward charge asymmetry in e^+e^- annihilation into muon pairs (called a dimuon). The charge asymmetry is defined as:

$$A_{\mu\mu}(\theta) = \frac{N_{\mu^-}(\theta) - N_{\mu^-}(\pi-\theta)}{N_{\mu^-}(\theta) + N_{\mu^-}(\pi-\theta)}$$

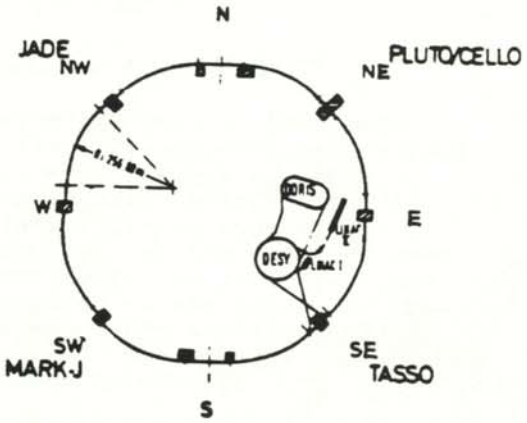

Figure 1
The PETRA storage ring and the four experimental groups.

where $N_{\mu^-}(\theta)$ is the number of μ^- counted in the solid angle $d\Omega$ about the direction (θ,φ). Figure 2 shows how the angles are defined in the reaction. Since the statistics of the experiment are still too small to make a precise asymmetry measurement in each θ bin, the asymmetry quoted is integrated over angle:

$$A_{\mu\mu} = \frac{N(\theta<\frac{\pi}{2}) - N(\theta>\frac{\pi}{2})}{N(\theta<\frac{\pi}{2}) + N(\theta>\frac{\pi}{2})}$$

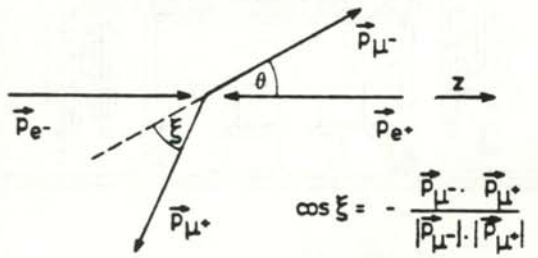

Figure 2
Schematic of the experiment. The angle θ is the angle the negative muon makes with the direction of the electron. The acollinearity angle is ξ.

Figure 3 shows a side view of the MARK J detector. In this experiment, the forward muon trigger counters and chambers (labled E and R respectively) were used to measure the asymmetry. These counters and chambers not only detect charged particles, but can be used to locate the position of the track of the particle as it passes through the detector. Together with the magnetic field, they are used to determine the momentum of the muons.

An experiment that used the MARK J detector had previously reported (3) a charge asymmetry of $(-10.4 \pm 2.1)\%$ in the angular range $0 \leq |\cos\theta| < 0.8$ at E_{cm} = 34.6 GeV. This compares favourably with the Glashow-Salam-Weinberg (GSW) (4) theoretical prediction of $(-8.6 \pm 0.2)\%$ for $\sin^2\theta_\omega = 0.23$ (5). In the present work, the forward E counters and R chambers are included. This extends the angular range to $|\cos\theta| < 0.9$. The GSW unified electroweak theory predicts a maximum charge asymmetry at small angles. By including the smaller angles, the validity of the theory could be tested with greater precision.

THEORETICAL BACKGROUND

The reaction $e^+ + e^- \rightarrow \mu^+ + \mu^-$ proceeds through both a photon and a Z^0 exchange. The corresponding lowest order Feynman diagrams are shown in Figure 4. The photon exchange represents the pure electromagnetic process and the Z^0 exchange the pure weak process. Using Bjorken and Drell (6) notation, the effective Lagrangian for this reaction is:

$$\mathcal{L}_{eff} = -\bar{\psi}_e\gamma^\nu(g_v+g_a\gamma^5)\psi_e Z_\nu - \bar{\psi}_\mu\gamma^\nu(g_v+g_a\gamma^5)\psi_\mu Z_\nu$$
$$- e\bar{\psi}_e\gamma^\nu\psi_e A_\nu - e\bar{\psi}_\mu\gamma^\nu\psi_\mu A_\mu$$

where g_v and g_a are the vector and axial vector couplings of the Z^0 to the lepton field, Z_ν represents the weak field, A_ν the electromagnetic field, γ^ν are the Dirac γ matrices and ψ the particle wave functions. To the lowest order, the differential muon pair production cross section is:

$$\frac{d\sigma}{d\Omega} = \frac{\alpha^2}{4s}\left[F_1 (1+\cos^2\vartheta) + F_2 \cos\vartheta \right]$$

where,

$$F_1 = 1 + 8sgg_v^2\chi + 16s^2g^2(g_a^2+g_v^2)^2\chi^2$$

pure QED; pure weak; electroweak inteference

$$F_2 = 16sgg_a^2\chi + \mathcal{O}(\chi^2)$$

$$\chi = M_Z^2 / (s - M_Z^2)$$

$$g = G_F/8\sqrt{2}\pi\alpha = 4.49\cdot10^{-5}\ GeV^{-2}$$

The asymmetry part of the cross section is the term proportional to $\cos\theta$. The term F_2, which is due to the weak-electromagnetic interference, is the major factor giving rise to the charge asymmetry. At the energies used in this experiment, the pure weak term is small compared to the pure QED term. The interference term amplifies the effect of the Z^0, producing a forward-backwrd asymmetry:

$$A_{\mu\mu}(\theta) = 7\times10^{-4}\, s\, g_a^2\, \chi \cos\theta / (1 + \cos^2\theta)$$

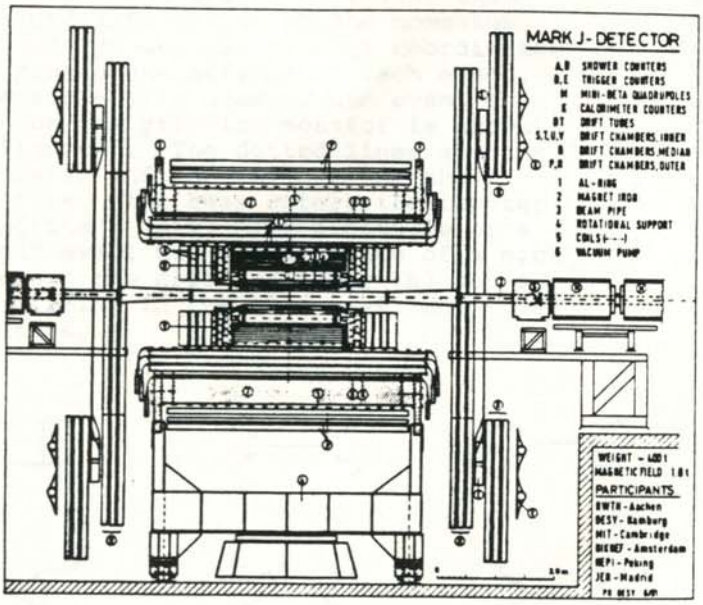

Figure 3
A side view of the MARK J detector. Note the vertical E counters and R chambers.

This theoretical asymmetry is plotted as a function of the angle θ in Figure 5.

These values have to be modified to take into account radiative corrections from QED. Feynman diagrams of order α^3 (shown in Figure 6) also cause a charge asymmetry, but of the opposite sign. The effect of these are shown in Figure 7. The theoretical value of the charge asymmetry is then:

$$A_{\mu\mu} = A^{GSW} - A^{QED}$$

Where A^{GSW} is the theoretical value and A^{QED} is the correction from QED processes.

Apart from the direct observation of the Z^0 (7), the precise determination of the charge asymmetry due to electro-weak interference is the most important verification of the ideas of the unified electroweak theory.

EXPERIMENTAL METHOD

As seen in Figure 5, the weak asymmetry is maximum at the smallest angles. The forward counters were installed on the MARK J detector to push the acceptance down to $|\cos\theta| < 0.9$ and thereby test the theory at smaller angles where the asymmetry is larger.

Muon pair events were selected according to certain criteria (8). To study the events in the extended angular range offered by the E counters, an off-line program selected those events that have E counter hits. An interactive graphics routine was used to examine the selected individual events. An outline of the MARK J detector was also plotted on the same screen. In this manner, we could "see" the track of the selected particles through the detector. The routine also

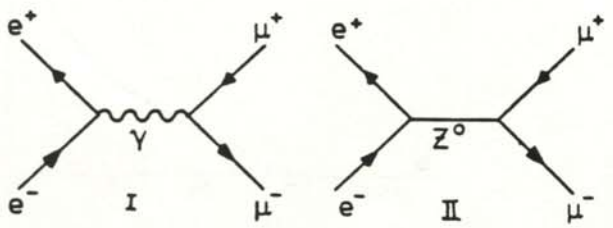

Figure 4
Lowest order Feynman diagrams for a γ and a Z^0 exchange.

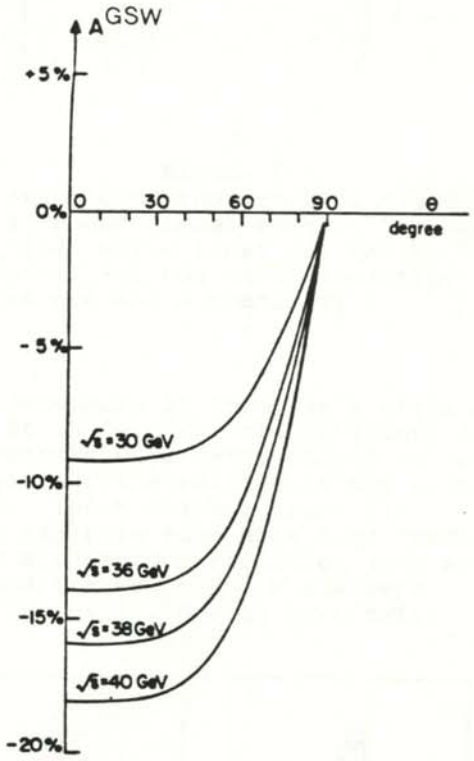

Figure 5
Forward-backward charge asymmetry for the weak interaction from the GSW theory.

provided an interactive monitor that supplied information on the momentum fit, energy deposition, hit coordinates and many other details of each event. An example of a good dimuon event as seen on the graphics monitor is shown in Figure 8. The dotted lines are the R chambers, and the solid lines the E counters. The beam enters the counter along the z axis. The signature of a "good" event was the presence of a nice track in the drift chambers (R) and a good timing in the time-of-flight counters.

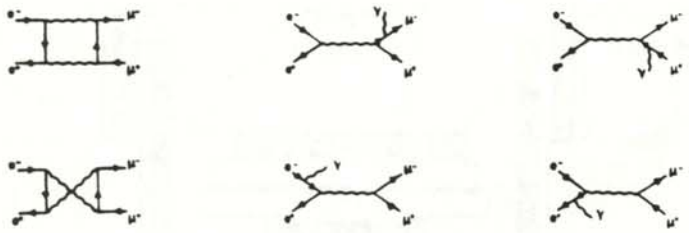

Figure 6
Order α^3 Feynman diagrams for asymmetry causing reactions.

A problem that was unique to the E counters and needed investigation was the background due to synchrotron radiation. The E counters are not well shielded from the mini-β quadrupoles at the entrances of the electron and positron beams. During a run at 41 GeV, at a certain constant interval, all trigger requirements were

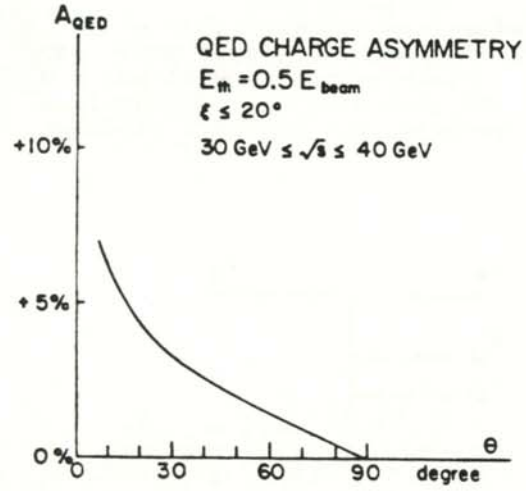

Figure 7
Charge asymmetry from QED.

suppressed and the gate opened when the beams collided to record all the hits with completely no bias. A scanning of these "beam gate" events showed an average of 9 random hits per good event. This poses a serious problem because the synchrotron radiation hits which occur in random coincidence with muon hits from the dimuon production ruin the timing.

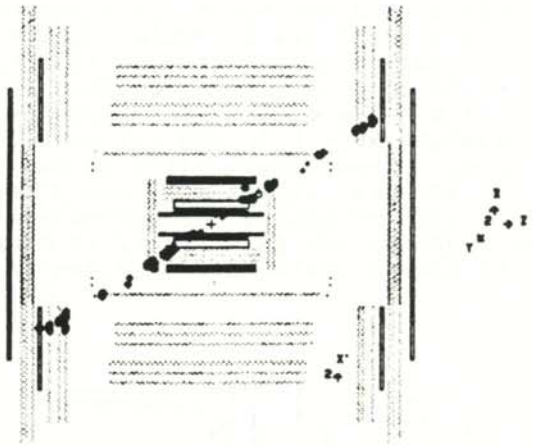

Figure 8
An example of the graphics display of a "good" dimuon event. The vertical solid lines are the E counters and the vertical dotted lines are the R chambers.

To determine if this was a serious problem at 34 GeV, the tracks fitted in the R chambers were extrapolated to the E counters and the postion of the hits compared. The R chamber track fit helps to separate muon hits from random hits, as synchrotron radiation does not leave good tracks in the R chambers because of its low energy (typically

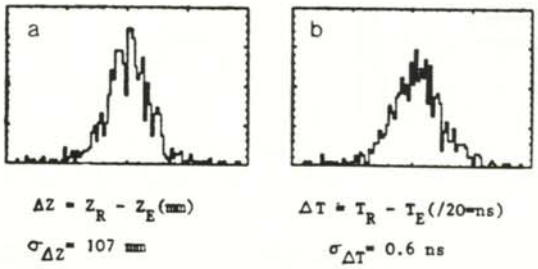

Figure 9
Timing and spatial resolution of the E counters. These results indicate that synchrotron radiation is not a problem at 34 GeV.

1 MeV.) Figure 9a shows the comparison of the hit position from the E counters and the R chambers. Figure 9b is a comparison of the timing from the E counter and that calculated from the positions reconstructed from the tracks in the R chambers. They showed that the E counters have pretty good timing and spatial resolution. It is apparent from these histograms that the level of the synchrotron radiation effect was not very serious at 34 GeV, the energy

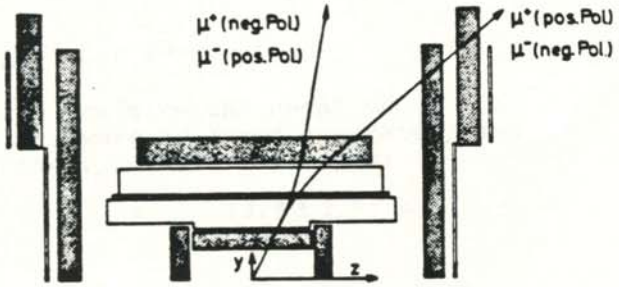

Figure 10
Diagram of the MARK J detector showing the effect of the magnet polarity on the trajectory of the charged muon. The vertical hatched detectors are the R cambers. The horizontal solid detectors are the D counters.

at which this experiment was run. The effects, however, are noticeable at 40 GeV.

DATA ANALYSIS

To calculate the charge asymmetry, one needs simply to count the number of μin the forward and backward hemispheres. To this end, the toroidal magnetic field of the detector acts as a charge indentifier. The curvature of the muon trajectory tells the momentum as well as the charge of the muon. Figure 10 shows how the charge of the muon is determined by the polarity of the magnetic field.

One has to have a way of eliminating events due to two photon processes such as those shown in Figure 11 and events due to hard photon bremstrahlung. Radiative events tend to have high values of acollinearity (see Figure 2) and two photon events have a small muon momentum. By applying a momentum cut of $P\mu/E_b > 0.5$ and an acollinearity cut of $\xi < 20$ degrees, one can separate events due to lowest order γ and Z^0 exchange from the radiative and two photon events. Figure 12 illustrates the momentum and collinearity cut applied. Figure 13

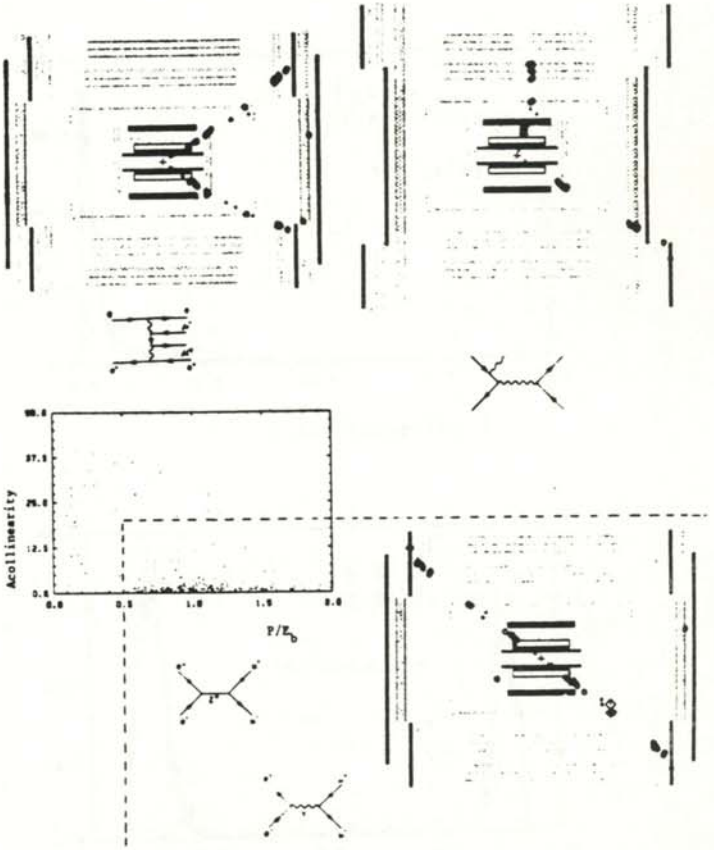

Figure 12
Momentum P_μ and acollinearity ξ cuts.

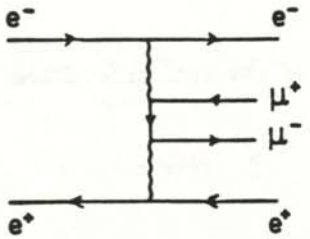

Figure 11
Feynman diagram of a two photon process.

illustrates the momentum and acollinearity distributions before and after the cuts.

Another potential problem is the inherent asymmetry of the MARK J detector itself. One of the nice features of the MARK J is that the magnetic feld polarity can be switched. One can thus gather data at both polarities. The detector asymmetry can then be compensated according to the following scheme:

$$A^{+} = A + A^{DET}$$

$$A^{-} = A - A^{DET},$$

thus

$$A = (A^{+} + A^{-})/2$$

$$A^{DET} = (A^{+} - A^{-})/2.$$

Data with positive and negative polarities were analyzed separately and the asymmetry determined to be:

$$A^{T} = (-13.3 \pm 3.5) \%$$

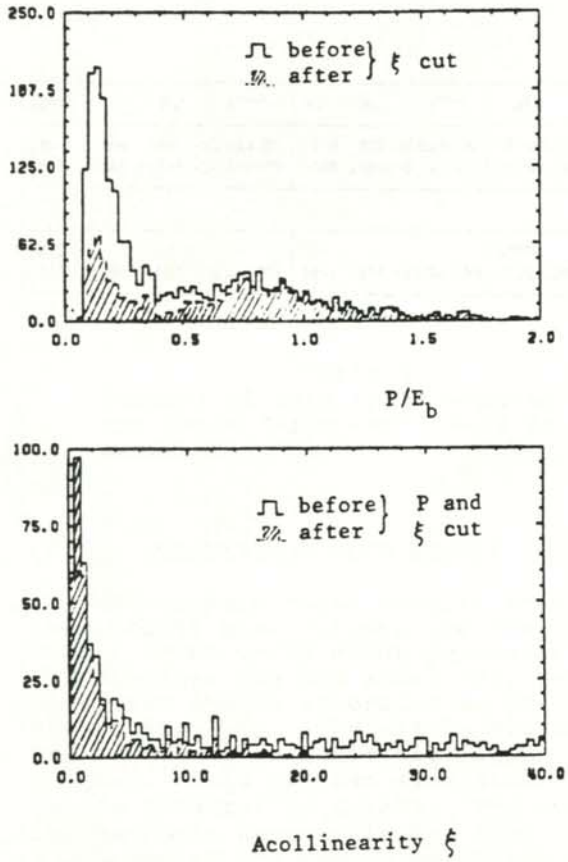

Figure 13
Momentum and acollinearity distributions before and after the cuts.

$$A^{DET} , = (-6.7 \pm 3.5) \%.$$

The charge asymmetry (A^{T}) measured above is the total asymmetry, including $A_{\mu\mu}$ and A^{QED}. The error associated with

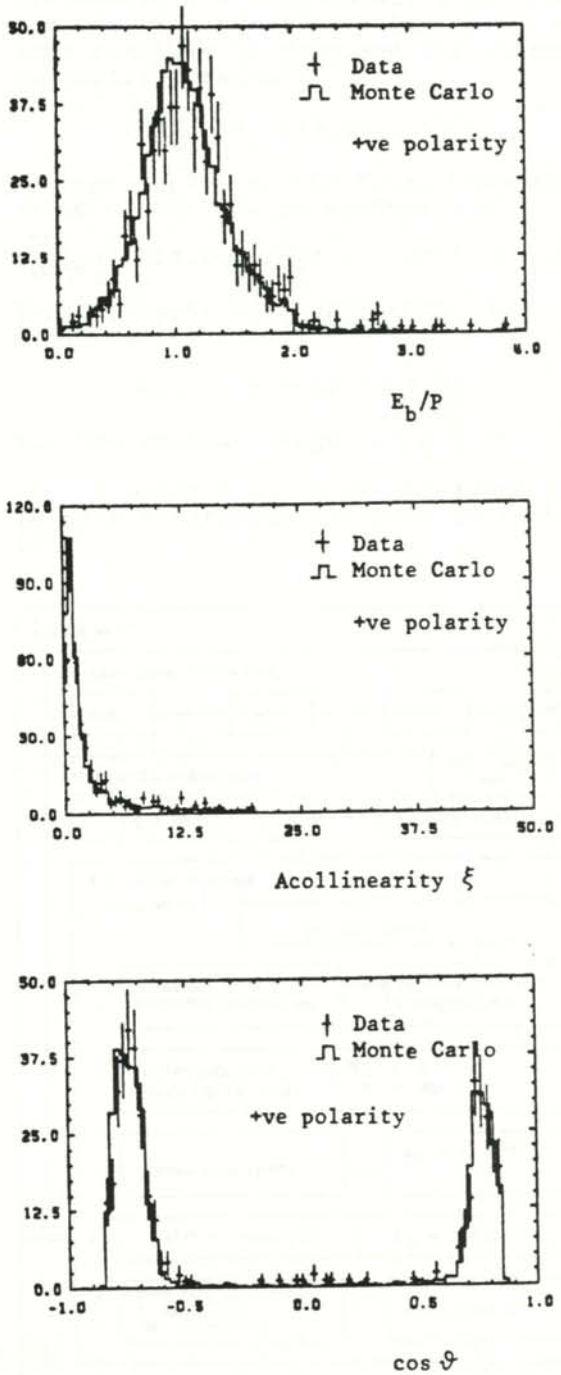

Figure 14
Comparison of real data and Monte Carlo generated data on the momentum distribution, the acollinearity distribution, and the forward-backward asymmetry.

the asymmetry is given by:

$$\sigma = \left[(1 - A)/(N_f + N_b)\right]^{\frac{1}{2}}$$

where N_f and N_b are the number counted in the forward hemisphere and backward hemisphere respectively. The results are summarized in Table 1.

An attempt was made to do the same analysis on those events that do not involve more than one D counter (the horizontal counters in Figure 10). They are events in the extra angular range covered by the E counters. Only a small percentage of the events are of this type. Trying to fit the momentum of the muon led to serious problems. The muon only passes through a small section of the magnet, so the momentum resolution is insufficient to determine the charge of the muon. This adds to the problem of determining the asymmetry from a small data sample.

Data	N_f^+	N_b^+	A^{POL+}	N_f^-	N_b^-	A^{POL-}	A^T	A^{DET}
Raw	164	246	-20.0±4.8%	176	201	-6.6±5.1%	-13.3±3.5%	-6.7±3.5%
M.C.	1248	1846	-19.3±1.8%	1485	1580	-3.1±1.8%	-11.2±1.3%	-8.1±1.3%
M.C. QED	1454	1587	-4.4±1.8%	1691	1374	+10.3±1.8%	$A^{QED}_{\mu\mu}$ +3.0±1.3%	-7.4±1.3%

Table 1
Summary of data (both experimental and Monte Carlo (MC)) used in this experiment.

COMPARISON WITH THEORY

To compare these results with theoretical predictions, one starts with a Monte Carlo event generator that incorporates the GSW model (9), and generates events according to the theory involved. The events are then fed through a detector simulation program. This program simulates the entire detector in detail. The events in the Monte Carlo file are then subjected to the same cuts as the real data. Figure 14 shows a comparison of real data and Monte Carlo generated data. It is evident that they are in good agreement. The Monte Carlo data gives an asymmetry of:

$$A^{MC}_{\mu\mu} = (-11.2 \pm 1.3)\%$$

To convert this to the weak charge asymmetry, one has to calculate and subtract the contribution to it from QED. Another Monte Carlo file is generated that includes only QED processes, one with negative polarity and one with positive polarity. The same analysis is done and the charge asymmetry obtained.

$$A^{MC}_{QED} = (+3.0 \pm 1.3)\ \%$$

We thus arrive at the final theoretical value of the charge asymmetry of:

$$A^{MC}_{GSW} = (-14.2 \pm 1.8)\%\ ,\quad \sin^2\theta_\omega = 0.23$$

This compares favorably with the experimental value:

$$A_{\mu\mu} = (-16.3 \pm 3.7)\ \%$$

for the angular range $0.5 < |\cos\theta| < 0.8$

A block diagram of the steps taken in this experiment is shown in Figure 15.

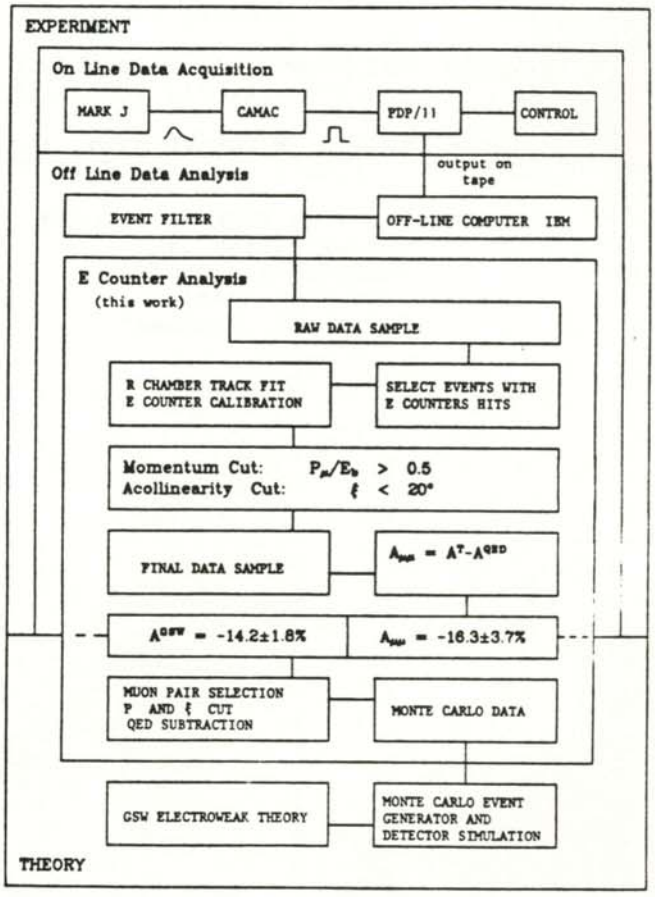

Figure 15
Block diagram of the steps taken in this experiment.

CONCLUSIONS

The forward counters of the MARK J detector have been studied and found to have good resolution. The charge asymmetry of the reaction $e^+ + e^- \rightarrow \mu^+ + \mu^-$ in the angular range in common to the forward and the side counters compares well with the GSW model prediction. An effort was made to extend the experiment to the extra angular range offered by the forward counters, but a lack of bending power in the forward region made it hard to determine the charge of the muon with the same reliablility as in the central region.

It should be emphasized again that the determination of charge asymmetry provides a test of the GSW theory apart from the direct observation of the intermediate vector bosons themselves. In principle, the charge asymmetry allows one to test the relationship between the mass of the intermediate bosons and the vector and axial vector weak couplings in more detail as they are all related through the unique parameter of the unified theory, viz. the Weinberg angle θ_ω.

The precise test of the GSW theory involves radiative corrections to the $W^\pm$ and Z^o masses, and $\sin^2\theta_\omega$. It is the self-consistency of all these basic parameters that will determine if the GSW theory is fundamentally correct. The determination of the charge asymmetry thus provides a test of the unified electroweak theory at a more quantitative level than just an identification of a particle.

REFERENCES

(1) The MARK J Collaboration, Phys. Rep. 63, 337 (1982).

(2) F. Hasert et al., Phys. Lett. 46B, 138 (1973).

(3) J.G. Branson, DESY 82-078, (1982).

(4) S. Glashow, Nucl Phys. 22, 579, (1961)
S. Weinberg, Phys. Rev. Lett. 19, 1264, (1967)
A. Salam, Elementary Particle Theory, H. Svartholm ed., Almquist and Forlag, Stockholm, 1968.

(5) θ_ω is the Weinberg angle. This parameter has to do with the relative strength of the electromagnetic and weak interactions.

(6) Bjorken and Drell, Relativistic Quantum Mechanics, McGraw-Hill Book Company, Inc., New York, 1964.

(7) The UA1 Collaboration, CERN-EP/83-73, (1983)
The UA2 Collaboration, recent results presented at the Cornell Conference (1983).

(8) B. Adeva et al., Phys. Rev. Lett., 48, 1701, (1982).

(9) F.A. Berends and R. Kleiss, Nucl. Phys. B177, 237, (1981).

FACULTY SPONSOR OF THIS PAPER
Dr. Harvey Newman
Physics Department
Caltech 256-48
Pasadena, CA 91125

MICROCOMPUTER ANALYSIS OF THE PHYSICAL PENDULUM *

Stuart C. Billette and Tim Folkerts
Physics Department
Central College
Pella, IA 50219

ABSTRACT

A microcomputer was used for data acquisition of the motion of a physical pendulum oscillating at various amplitudes. The pendulum was mounted on a ten turn potentiometer. The potentiometer acted as a voltage divider, giving an output proportional to the instantaneous angle of the pendulum. The microcomputer collected and stored the value of the voltage as function of time, which then was displayed on an oscilloscope. The period, as determined from the oscilloscope readings, was within 2% of the predicted period for all amplitudes up to 169 degrees.

INTRODUCTION

Often it is necessary to measure many closely spaced events to properly do an experiment. While manual techniques are possible, they lead to a large number of uncertainties that often vary from observer to observer. The fairly inexpensive microcomputer presents to the experimenter a way to standardize these measurements and at the same time obtain a greater degree of accuracy. The microcomputer also can collect and store data rapidly and present them for analysis later.

One application that lends itself well to microcomputer data acquisition is the measurement of the period of a physical pendulum. It is very difficult to measure the period of a pendulum with large amplitude accurately with a stop watch because after a few oscillations, damping reduces the amplitude significantly. It is possible to use a microcomputer with a transient recorder program and an oscilloscope to obtain an easily measurable trace of the pendulum's angular position as a function of time. This trace can be produced a number of times and shows very little deviation. Thus, the microcomputer allows the determination of the period with both a high degree of accuracy and reproducibility.

THEORY

A rigid body which is free to swing under its own weight about a fixed horizontal axis is known as a physical pendulum. An example of one is shown in Figure 1. O is the location of the axis of rotation. L is the distance between the center-of-mass and the axis of rotation. The motion is described by the second order non-linear

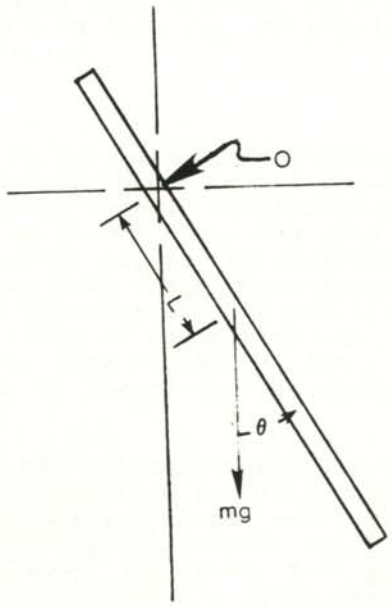

FIGURE 1
A physical pendulum oscillating about a fixed axis at O.

differential equation:

$$\ddot{\theta} + [mgL/I] \sin(\theta) = 0 \qquad [1]$$

where m is the mass of the pendulum and I is its moment of inertia about the axis of rotation.

For the case of small oscillations, the equation can be linearized by making the substitution:

$$\sin\theta \simeq \theta \qquad \theta \ll 1 \qquad [2]$$

This now is the equation of a simple harmonic oscillator with period given by:

$$T = 2\pi\sqrt{I/mgL} \qquad [3]$$

Thus the period is the same as that of a simple pendulum of length I/mL.

The pendulum used in this experiment was a thin rod, 1.00 meters in length with a few regularly spaced small holes drilled so that the axis of rotation could be changed. To calculate the period, it was first necessary to determine the moment of inertia of the object.

The moment of inertia of a long thin rod, rotating about its center, is:

$$I_{cm} = mr^2/12 \qquad [4]$$

where m is the mass of the rod and r is its length. Using the parallel axis theorem, the moment of inertia of the rod about an axis perpendicular to the rod and L meters from the center-of-mass is given by:

$$I = mr^2/12 + mL^2 \qquad [5]$$

This result is used to determine the period for any rotation point of the rod for small angles.

One cannot find an exact solution to the equation of motion for large angles. The solution can be determined in terms of elliptic integrals of the first kind. A computer program was written to numerically evaluate the integrals (1) and the results compared with experimentally measured values (2). A more detailed theory of the physical pendulum can be found in the text on Analytical Mechanics by G.R. Fowles (3).

PROCEDURES AND RESULTS

The physical pendulum was attached to a precision ten turn potentiometer across which was placed a regulated adjustable voltage supply. A SYM-1 microcomputer (4) was attached to the potentiometer to receive and read the voltage. The voltage was then converted by the computer to a digital number between 0 and 128. The system could store up to 256 values. The SYM-1 accepts voltages in the range 0 - 5 volts. To get full scale readings for amplitudes of 30 degrees, a regulated power supply capable of producing a voltage up to 400 volts was used to set the potential across the potentiometer. The output from the microcomputer was then fed directly into an oscilloscope where a trace of the motion was displayed. (see Figure 2). The schematic of the circuit is shown in Figure 3.

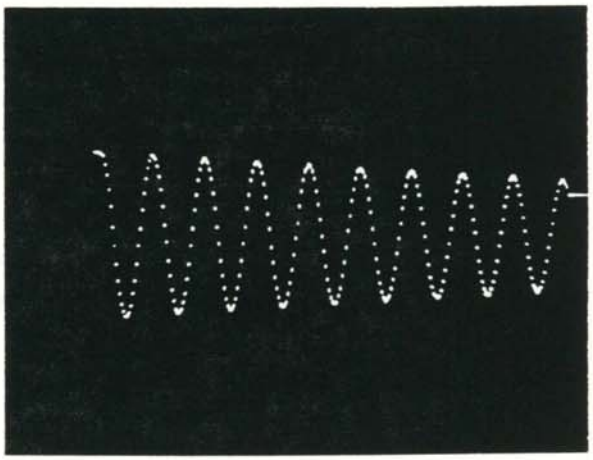

FIGURE 2
Typical oscilloscope trace of angle vs time for the physical pendulum.

The potentiometer body was turned so that the voltage read 2.5 volts at the rest position (angle = 0 degrees) and the voltage at maximum deflection was just under 5.0 volts (full scale reading on the SYM-1). This means that the full scale of the microcomputer voltmeter was utilized, making the beginning and end of each period more ascertainable. The time interval between successive readings was made as short as possible (0.02 sec.) to better fix the beginning and end of one swing. A set of results are shown in Table 1.

The values in Table 1 are the average of three trials with L = 0.195 meters. Trials run with different values of L yielded similar results. To minimize the error due to damping at angles greater than 90 degrees, the time for the first half-period was taken and then doubled. Any amplitude over 90 degrees reported in Table 1 was the average of the initial deflection and the maximum deflection one-half period later. It was discovered that the damping had no noticeable effects on the results for angles less than 90 degrees. Due to the limitations of our apparatus and the damping, the largest amplitude we were able to measure using this technique was 169 degrees (the average of 180 degrees and 158 degrees).

Amplitude	Predicted Period	Experimental Period	Percent Difference
5°	1.58 s	1.58 s	0.0%
10°	1.58 s	1.58 s	0.0%
20°	1.59 s	1.59 s	0.0%
30°	1.61 s	1.61 s	0.0%
40°	1.63 s	1.65 s	1.2%
50°	1.66 s	1.67 s	0.6%
60°	1.70 s	1.72 s	1.2%
70°	1.74 s	1.76 s	1.1%
80°	1.80 s	1.83 s	1.7%
90°	1.87 s	1.87 s	0.0%
99°	1.94 s	1.97 s	1.5%
108°	2.02 s	2.04 s	1.0%
118°	2.14 s	2.12 s	0.9%
128°	2.28 s	2.23 s	2.2%
136°	2.44 s	2.41 s	1.2%
145°	2.64 s	2.67 s	1.1%
154°	2.92 s	2.93 s	0.3%
163°	3.33 s	3.29 s	1.2%
169°	3.76 s	3.80 s	1.1%

TABLE 1
Results from a typical experiment. The length of the pendulum was 1.00 m. and L was 0.195 m. The values are averages for three different trials. The angles are the average amplitude for one-half of a period.

The experimental determination of the period was done to an accuracy of 2% for all angles. This also was true for other values of L. The error was largely due to inaccuracies in measuring amplitudes with a protractor.

The data experimentally verified a rather elaborate theory to a high degree of accuracy. The SYM-1, used as a rapid data collector, performed an experiment that would have been impossible to do with manually controlled equipment.

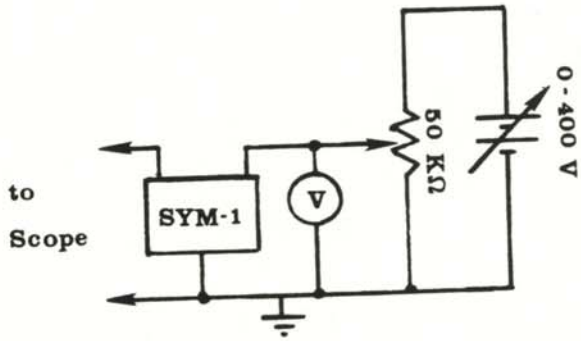

FIGURE 3
Schematic diagram of the circuit used to measure the period of a physical pendulum. The pendulum is attached to the 50 KOhm ten turn precision potentiometer.

REFERENCES

* This experiment was part of the Advanced Laboratory sequence at Central College.

(1) A copy of this program may be obtained by writing to the Physics Department at Central College, Pella, Iowa 50219.

(2) Values were also calculated directly from a table of integrals for an elliptic integral of the first kind. The computer program, however, was accurate to 0.1% and was much less time consuming.

(3) G.R. Fowles, Analytical Mechanics, 3rd Ed., Holt, Reinhart and Winston, New York, 1977, pp.199-200.

(4) SYM-1 microcomputer and accompanying transient recorder program information can be obtained by writing to Cambridge Development Laboratory, 36 Pleasant Street, Watertown, Maine 02172.

FACULTY SPONSOR OF THIS PAPER
Dr. Allen Moen
Physics Department
Central College
Pella, Iowa 50219

A COMPENSATED THERMOCOUPLE FOR MEASUREMENT OF THE CURIE TEMPERATURE

Andrew Degges
Physics Department
Guilford College
Greensboro, NC 27410

ABSTRACT

An inexpensive thermometer for measuring the Curie temperature was designed and calibrated. Op-amp circuits were used to compensate for the nonlinearity and cold junction error in an economical Ch-Al thermocouple. Using this apparatus, the Curie temperature for nickle was found to be (311±3) C.

INTRODUCTION

An experimental study of the Curie temperature is a particularly appealing undergraduate laboratory topic as it provides the experimenter with physical insight into a quantum mechanical phenomena manifested on a macroscopic scale. Moreover, it teaches experimental finesse in the area of high temperature thermometry.

The Curie temperature is defined as the temperature at which the permanent magnetization of a ferromagnetic domain disappears. Ferromagnetism is an anomalous condition of extremely high magnetic susceptibility particular to certain transition and rare earth metals: the periodic triplet of iron, cobalt, and nickle; and the two rare earth elements, gadolinium and dysprosium. These have room temperature susceptibilities on the order of 10^5or greater, while normal metals are on the order of 10^{-4}.

The unusually high susceptibility in ferromagnets is due to the high degree of electronic spin alignment present in them. For large macroscopic regions (domains on the order of 10^{-5}m. on a side), the spins of the conduction electrons are aligned parallel to each other. The spin alignment is due to the quantum mechanical exchange energy. The requirement of an anti-symmetric wavefunction creates to distinct eigenstates. The difference in energy of these two states is the exchange energy. How the exchange energy causes the spin alignment can be seen the the following example.

Iron has six principle valence electrons located in the 3d orbital. This d orbital is only partially filled (it could hold ten electrons). If there were no difference in the energy between the eigenstates, one would expect the electrons to align themselves in the following manner: three with spin up, three with spin down. However, there is a difference in the energy between the two exchanged states, and the atom will try to minimize its energy. The atom, therefore, arranges itself with 5 of the electrons with parallel spins and only one antiparallel.

When such atoms are placed in a crystal, the width and population of the energy bands within a Brillouin zone will be strongly influenced by the exchange energy (if it is on the order of the Fermi energy). The Fermi energy of the arrangement with 5 electrons aligned and one opposed is higher than that with 3 aligned each way. However, the lower exchange energy more than compensates for the increase in the Fermi energy. In addition, the width of the 3d band has been broadened and a 3d-4s hybrid band has been created.(1) This hybridization of the band structure has a marked effect on the conductivity of the iron. Iron crystals with the electronic structure where 5 are aligned and only one anti-parallel will have a higher conductivity than those with three up and three down.

The energy difference between these two states is so small that it is possible to overcome the exchange

energy with the addition of thermal energy. The Curie temperature (usually on the order of a few hundred degrees Celsius) is the temperature at which the thermal energy overcomes the exchange energy and the band structure of the crystal reverts to the isotropic structure that has three electrons with spin up and three with spin down.

The connection between the electrical resistance of a material and the electron configuration due to ferromagnetism can be exploited to measure the Curie temperature. The conductivity of a pure metallic conductor is given by the Bloch-Grüneisen equation:

$$\rho[T] \propto (T/\theta_d)^5 \int_0^{\theta_d/T} \frac{x^5\, dx}{(e^x - 1)(1 - e^x)} \qquad (1)$$

where ρ is the resistivity at temperature T, θ_d is the Debye temperature and $x=\theta_d/T$. When one includes phonon-electron interactions, the relationship for the resistivity as a function of temperature becomes:

$$\rho[T] = \xi^{-1} m^*/n_f e^2 \qquad (2)$$

where ξ is the mean time between collisions, m^* is the effective carrier mass, n_f is the charge carrier density at the Fermi surface.(2)
If one measures the resistance of a ferromagnetic material, it should follow

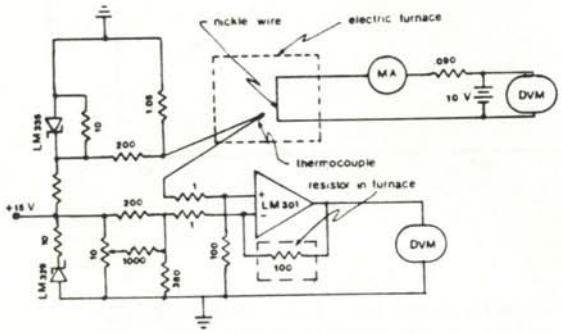

Figure 1
Schematic diagram of the compensation circuit. Note that the feedback resistor on the LM301 is placed in the oven near the nickle wire. All the resistances are in KOhms.

Equation 2 until it approaches the Curie temperature. At that temperature, the ferromagnet should display a higher resistivity than that predicted by Equation 2 because of the strange electron spin alignment. In this experiment, we make use of this phenomenon to measure the Curie temperature of a sample of nickle wire.

THE EXPERIMENT

We measured the Curie temperature of a sample of nickle wire by measuring its resistance as a function of temperature between room temperature and 400 C. Figure 1 is a schematic representation of the experimental setup. This is essentially the same technique as outlined by Kamam, et.al. (3) with one important exception. They used a rather expensive platinum-platinum rhodium thermocouple with a cumbersome cold junction compensation apparatus. We designed a less expensive temperature measuring system.

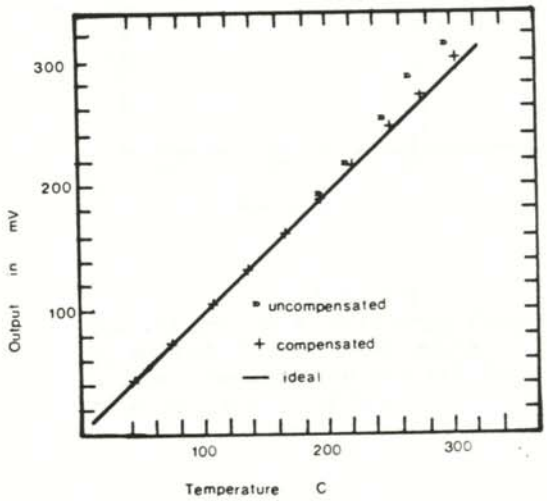

Figure 2
Calibration curve for the thermocouple. Notice how the compensation circuit brings the output of the J-Type thermocouple close to that expected for an ideal thermocouple.

There are two major problems that arise when thermocouples are used to measure temperatures over a wide range. The first problem is one of nonlinearity at high temperatures (T> 275 C). All thermocouples have regions where their response curves differ from a straight line due to Seeback emf's (4). It is possible to find

thermocouples with a large linear region, but in general they are very expensive. A cost effective was of dealing with this problem is to resort to signal shaping with an operational amplifier. If the feedback resistor is in thermal contact with the thermocouple, its resistance will increase for a corresponding increase in temperature. This has the effect of compensating for the nonlinearity of the thermocouple response. In our experiment, this was done with the LM 301 chip (see Figure 2).

The second problem is that of cold junction compensation. When the thermocouple is terminated to a meter or amplifier, it creates two more thermocouple junctions. Each of these will produce a spurious voltage proportional to the ambient temperature. The usual method of eliminating this requires immersing the terminals in an ice-water bath. We used a temperature sensing zener diode

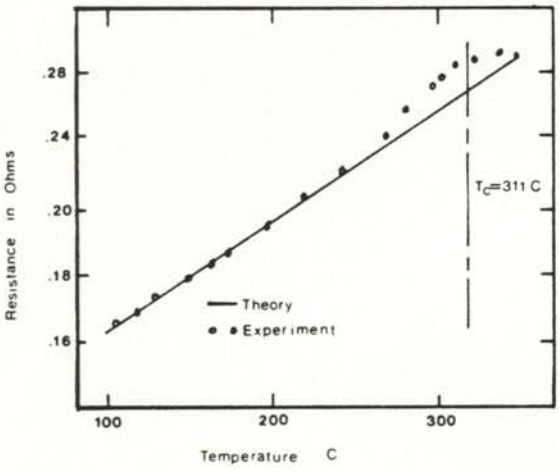

Figure 3
Measurement of the resistance of a 2.5 cm. long piece of nickle wire as a function of temperature. Note how near the Curie temperature the data points leave the line expected of a pure metal.

and a precision voltage reference to do the same thing. The LM 335 chip in Figure 1 regulates a voltage to counter the spurious junction voltage.

Figure 2 is a plot of the voltage produced by our compensated J-type Chromel-Aluminum thermocouple. Also plotted on this graph is the expected behavior of the thermocouple according to the literature (5).

We used this compensated thermocouple to measure the resistance vs temperature for a 2.5 cm. long sample of nickle wire. Results of this are shown in Figure 3. To find the Curie temperature, we subtracted the measured resistances from the ones predicted by Equation 2. This is shown in Figure 4. The Curie temperature is the peak of this curve.

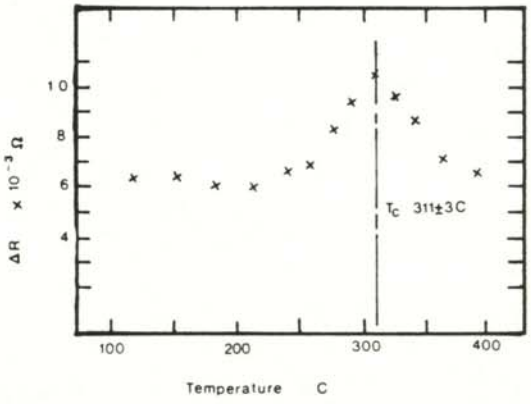

Figure 4
Deviation in resistance from that expected of an ideal metal. The Curie temperature should be the peak of this curve.

CONCLUSIONS

The use of low cost integrated circuits eliminates many of the problems associated with high temperature thermometry. This compensated thermocouple gave valid readings that allowed us to measure the Curie temperature of nickle. Our value of 311±3 C is within one standard deviation of the accepted value.

REFERENCES

(1) Sproull, R.L., and W. A. Phillips, Modern Physics, 3rd Ed., John Wiley & Sons, New York, 1980.

(2) Dekker, A.J., Solid State Physics, MacMillan, New York, 1963.

(3) Kamal, R., S. Sikri, and B.R. Sood, Am. J. of Phys., 51, July, 1983, p. 631.

(4) Temperature Measurement Handbook, Omega Engineering, Inc, 1984, p. T-11.

(5) Ibid. p. T-38.

FACULTY SPONSOR OF THIS PAPER
Dr. Rexford E. Adelberger
Physics Department
Guilford College
Greensboro, NC 27410

THE COMPOSITION OF INTERPLANETARY ENERGETIC CHARGED PARTICLE FLUXES DURING SOLAR MINIMUM

Joseph C. Shields
Department of Physics and Astronomy
University of Kansas
Lawrence, KS 66045

ABSTRACT

Data from the Johns Hopkins University Applied Physics Laboratory Charged Particle Measurement Experiment aboard IMP 8 was used to study particle flux composition near the earth during the 1974-1977 solar minimum. Daily-averaged particle count rates were used to determine the H/He and He/(C,N,O) composition ratios. These were sorted into three categories of activity: periods of flare activity; periods of non-flare non-quiet time; and quiet time. The three data subsets showed distributions of composition ratios that were markedly different from each other. In general, the H/He and He/(C,N,O) ratios had higher values during non-quiet, non-flare times than during quiet times. Flare particles showed a large variability in relative composition. The results of this study are consistent with previous compositional studies of the interplanetary medium that have been conducted for shorter periods of time. At least three distinct sources of these energetic particles are indicated by the differing compositions.

INTRODUCTION

The composition and energies of particles found in the interplanetary medium near the earth are influenced by a variety of solar phenomena such as flares and corotating regions. The study of the characteristics of these particles has provided information on some of the processes underlying these solar phenomena. Such studies may ultimately help answer questions about the structure and evolution of the sun and other stars.

The most dramatic and well-known solar active phenomena are flares, which often include eruptions of particles that are projected out of the solar corona at high energies. Flares vary greatly in size and structure. Their energy storage and accelerating mechanisms are not fully understood. Solar flares exhibit combinations of X-ray, microwave and radio bursts associated with varying degrees of mass ejection. Flares considered in this study are limited to those which produce noticeable increases in particle flux near the earth. These are classified as "particle events".

Corotating interplanetary regions represent another major source of interplanetary medium variation. Corotating regions are the outward extensions of active areas on the sun's corona that have a solar wind and magnetic structure causing interplanetary interactions of fields and particles which may result in particle confinement and acceleration. These regions follow the regular rotation of the sun's surface (hence "corotate") and may have long lifetimes. Corotating regions produce a cycling pattern of particle fluxes at the earth as the sun rotates every twenty-seven days. Corotating regions can produce particle fluxes comparable to those caused by flares, but the particles are generally less energetic. Both solar flares and corotating regions increase in number during maximum years of the sun's eleven year cycle of activity.

The study of particle fluxes that originate in solar activity is important for a number of reasons. Ions that interact with the earth's magnetic field and the outer atmosphere are responsible for geomagnetic effects such as aurorae and magnetic storms. They may also have important meteorological consequences. Solar flare produced particles are also important indicators of the chemical,

nuclear and thermal processes that take place in the sun. By examining the interplanetary debris of these processes, we may learn more about how they differ in time and place in the sun. A better understanding of these phenomena may lead to a more complete theory of solar and stellar evolution.

Particle flux composition at low energy has previously been studied in solar flares (1) and corotating regions (2). Attempts have been made to categorize the composition of the interplanetary medium during short intervals of "quiet time" (3). A few studies sought to describe composition during longer selected time periods (4). While detailed studies have been carried out for special categories and short periods of activity, none have attempted to describe in any comprehensive way the compositional features of the medium for time scales of several years.

This paper discusses long-term aggregate characteristics of the low energy interplanetary particle composition as measured by the Johns Hopkins University Applied Physics Laboratory (JHU/APL) experiment on IMP 8 during the years 1974-1977. We found that interesting comparisons can be made with the H/He and He/(C,N,O) composition ratios as determined for quiet time, non-flare non-quiet time, and the intervals of flare activity during this solar minimum period. The results of this study indicate that distinct compositional distributions may be favored for each of these categories of interplanetary particles.

DESCRIPTION OF THE EXPERIMENT

Data for this study were obtained from the JHU/APL Charged Particle Measurement Experiment (CMPE) on board the Explorer 50 (IMP 8) spacecraft which was launched on October 26, 1973. The experiment utilizes the proton-electron telescope (PET) to determine numbers of incident particles at various energies. A schematic representation of the PET detector assembly is shown in Figure 1 (5). D1 and D2 are silicon surface barrier detectors, and D3 is a lithium-drifted silicon detector. The plastic scintillator cup acts to eliminate counts from particles that stray from the trajectory within the detector's 45° angle of view. Daily average count rates were used in this study. The particle flux (I) can be calculated from the count rate (R) using the detector's geometrical factor G = 1.51 cm^2 str. according to the relationship I = R/G.

When an incident particle enters the assembly, the detectors make a combination of energy loss measurements depending upon the particle's speed and charge. These measurements are interpreted according to logic conditions that sort the aggregate particle counts into various channels. Each channel has an experimentally pre-determined passband. Passband information for the four data channels used in this study is given in Table 1.

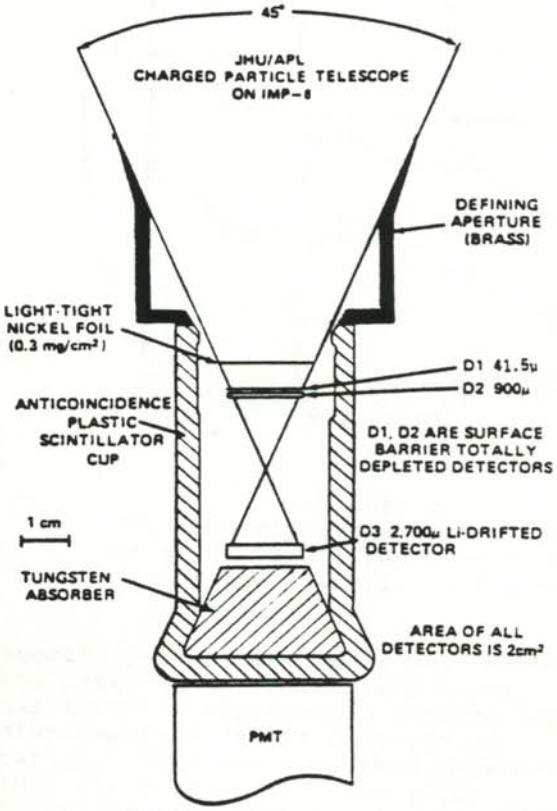

Figure 1
Cross-sectional view of the JHU/APL charged particle telescope.

OBSERVATIONS

The period between day 300, 1974, and day 200, 1977, was taken to be a data set characterizing solar minimum conditions. Composition ratios of H/He and He/(C,N,O) were calculated for this

period using data from channels P4, A3, Z1 and Z2 (6). Days during which known solar flares had a clear impact on the particle fluxes were removed from this data set and considered separately. Figure 2 is an example of a time series plot of proton, alpha and medium nuclei fluxes arising from a 1B flare of April 29, 1976, at heliocentric coordinates S08 W46 (McMath region #14179). This particle flux exhibited the typical features of solar flare events: abrupt onset; rapid rise and gradual decay. Many events exhibited much less regular features and a more complicated time structure.

Periods of maximum activity during the eleven year solar cycle have successive and often overlapping times of solar flare activity and active region corotation. These can be particularly difficult to distinguish and identify. The largest particle events are generally not difficult to identify because the resulting bursts of high energy particles (>200 MeV) are

	PASSBAND NAME			
SPECIES	P4	A3	Z1	Z2
HYDROGEN	2.00 - 4.60	-----	-----	-----
HELIUM	1.80 - 2.20	1.80 - 4.20	-----	-----
CARBON	3.15 - 3.30	3.15 - 3.90	0.82 - 1.70	1.70 - 3.15
NITROGEN	3.30 - 3.50	3.30 - 3.90	0.70 - 1.45	1.45 - 3.30
OXYGEN	-----	3.55 - 3.90	0.64 - 1.30	1.30 - 3.55
NEON	3.55 - 3.75	3.55 - 4.25	0.54 - 1.05	1.05 - 3.55
MAGNESIUM	3.55 - 3.75	3.55 - 4.25	0.46 - 0.89	0.89 - 3.55
SILICON	-----	3.85 - 4.25	0.46 - 0.89	0.89 - 3.90
IRON	3.90 - 4.15	3.90 - 4.55	0.22 - 0.42	0.42 - 3.90

Table 1
Passband data (Mev/Nucleon) for the IMP 8 spacecraft.

rarely seen at any other time. In contrast, lower energy flares are less clearly identifiable in time profile and exhibit more variation in composition (4).

In this study, flare days were identified using lists of particle events compiled for this period (7,8). Daily averages were removed from the composite data for days exhibiting increased particle flux that clearly could be correlated to events cited in these publications. The residual data set was assumed largely to be free of counts of particles of flare origin. Quiet time was defined to be those days in which the daily average alpha particle rate (channel A3) was less than 3.98×10^{-4} counts/sec. This

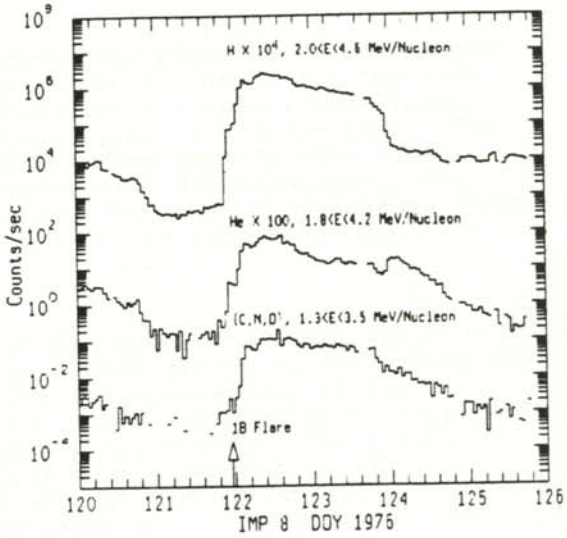

Figure 2
IMP 8 hourly-average count rates of H, He, and (C,N,O) particles during the 29 April 1976 event.

seemingly arbitrary value was chosen on the basis of the relatively clear partition it represented between two distributions of the composition ratios. When the data were separated into flare time (FT), non-quiet non-flare time (NQNF) and quiet time (QT), the H/He and He/(C,N,O) ratios fell into three fairly distinct ranges of values (see Figure 3). Both ratios showed higher ranges of values for NQNF than for QT. Details of the distributions such as the mean and standard deviations of the fluxes are shown in Table 2.

H/He Ratios

The NQNF distribution is particularly striking in its sharp, near Gaussian appearance on the logarithmic scale centered about a ratio = 29. This narrow distribution indicated that the H/He ratio favored a limited band of values for active non-flare times.

While QT displayed a broader distribution of H/He values than NQNF,

the majority of QT H/He ratios were relatively low. The distinct character of the quiet and the non-quiet portions of non-fare times was evident in the production of a double peaked composite H/He ratio (Figure 4). Flares at solar minimum produced a relatively broad and flat distribution. While flares exhibited highly variable composition ratios, they were clearly responsible for the highest values found in the composite distribution.

He/(C,N,O) Ratios

He/(C,N,O) composition ratios

Data set	Flare	Non-flare,Non-quiet	Quiet	Total
H/He:				
No.Days	130	301	493	924
Mean	95.3	33.2	18.0	33.8
Median	40.6	28.5	10.8	19.9
Stan.Dev.	139.	26.0	29.7	63.9
2/3 Range	12.3-159.	18.2-41.7	5.67-25.6	6.90-40.3
Tot.Range	4.02-744.	0.133-237.	2.14-452.	0.133-744.
He/(C,N,O):				
No.Days	132	301	493	926
Mean	36.8	67.1	15.3	35.2
Median	24.9	53.9	7.11	15.0
Stan.Dev.	52.0	63.5	30.3	52.2
2/3 Range	6.71-55.4	17.8-98.5	3.07-18.3	4.13-65.7
Tot.Range	0.742-472.	0.370-407.	0.435-284.	0.370-472.

Table 2
Statistics for Solar Minimum composition ratios.

showed a breakdown in distribution for non-flare times similar to those for H/He. As for the H/He ratio, the QT He/(C,N,O) composition was in general substantially lower than for NF time. Flares exhibited a broad range of composition ratio. Although the distributions for QT and NQNF composition appear narrower for H/He than for He/(C,N,O), they are similar in their effect of producing a double peak in the composite distribution (Figure 4). This feature is somewhat masked by the flare values.

CONCLUSIONS AND COMPARISONS WITH OTHER STUDIES

Particle events

The composition ratios calculated for the various times considered in this study are generally consistent

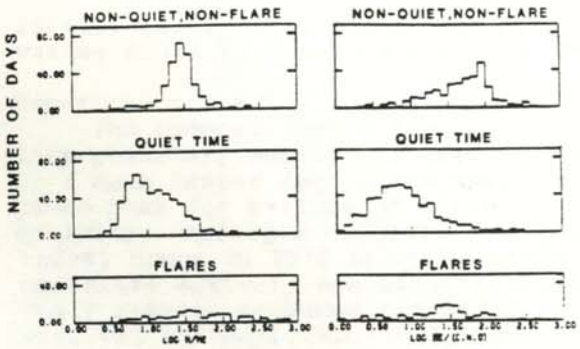

Figure 3
Histogram plots of solar minimum composition ratios for the time regimes: non-quiet, non-flare; quiet time; and flare time. The three time subsets show highly individual distributions. The flare events display a broad range of relative composition values.

with values cited elsewhere for similar periods. Composition at low energy has been studied extensively in flares, both for individual particle events and for larger aggregates. For a 1972 particle event, Bertsch et.al. (9) measured particle spectra to a lower energy limit of 10 MeV/nucleon. At this minimum energy, H/He was determined to be 24(+10,-8) (uncertainties reflect the counting statistics). Krimigis and Armstrong (3) studied a different 1972 particle event. Their results for (1.6 - 3.2) MeV/Nucleon particles produced H/He values ranging from 70 to 160. Armstrong and Krimigis (1) also studied a series of particle events that occurred during the years 1967 - 1968 and found that for particles with greater than 0.5 MeV/nucleon, H/He assumed values from 10 to 150. In another study of several particle events, Lanzerotti and Maclennan (13) examined seven particle events during 1967 - 1969 and found that at 2

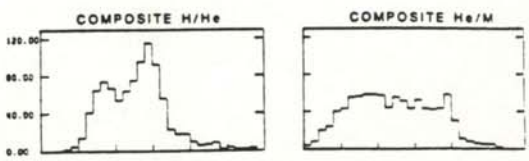

Figure 4
Histogram plots of composite solar minimum composition ratios.

MeV/nucleon, the median H/He ratio was 44(+33,-24). Mason et.al. (4) studied particle events that were active during 37 days in the years 1973 - 1977. Their results for 1.1 MeV/nucleon particles showed a mean H/He of 46, with two-thirds of the values falling between 13 and 121. In another study of 8 particle events selected from the same time period, Mason et.al. (11) found (.6 - 1.0) MeV/nucleon H/He value of 43(+116,-10). A particularly useful value for comparison is given in a review article by Gloeckler (10) in which seven earlier published sources were used to determine an average flare-time (1 - 20) MeV/nucleon H/He ratio of 66(+163,-59). In the study described in this paper, the median flare H/He ratio of 41(+119,-28) is consistent with these earlier values and ranges. (Uncertainties associated with median values computed in this study represent the limits of two-thirds of the total cases.)

Flare times

Values for flare-time He/(C,N,O) taken from the literature show a degree of consistency similar to those of the H/He ratios. Bertsch et.al. (9) measured a single-event He/(C,N,O) value to be 19(+6,-4) at 10 MeV/nucleon. By extrapolating the fit they used for composition ratio vs. energy/nucleon, an estimate of the He/(C,N,O) value of 16(+6,-3) can be made for particles with 2 MeV/nucleon. Krimigis and Armstrong (3) found in a single event that He/(C,N,O) had a mean of 23(+52,-8) for (1.6 - 3.2) MeV/nucleon particles. For multiple events, Armstrong and Krimigis (1) calculated a He/(C,N,O) ratio for particles of >0.5 MeV/nucleon of 20(+10,-10), where the uncertainty is due to flare-to-flare variations. Cook, Stone and Vogt (12) studied four flares in 1977-1978 at (4.6 - 15) MeV/nucleon and found the average He/(C,N,O) to be 45(+3,-3); composition ratio values ranged in their study from 28(+2,-2) to 93(+12,-12). An average value of He/(C,O) for the group of flares examined by Mason et.al.(4) was 45(+16,-22). Although nitrogen composition is not included in this ratio, it remains useful for comparison since nitrogen is typically a small influence on the magnitude of He/(C,N,O). The corresponding median value from Mason et.al (11) is He/(C,O) = 47(+10,-10). Gloeckler (10) gave a literature average value of He/(C,N,O) = 42(+58,-23) for particles with energy per nucleon between 1 and 20 MeV/nucleon. The flare-time median value of He/(C,N,O) we found of 25(+30,-18) is thus consistent with the values found in these earlier studies.

Non-flare times

The composition of the interplanetary medium has been studied to a much lesser degree for non-flare times than for periods of flare activity. Krimigis et.al.(3) examined thirty hours in 1972 in which flare and non-flare activity was largely absent. Their results produced ratios of H/He = 9(+2,-2) and He/(C,N,O) = 20(+30,-7), which are reasonably close our median quiet time ratios of H/He = 11(+15,-5) and He/(C,N,O) = 7(+11,-4). In the retrospect permitted by over eleven years of CPME data taking, the time interval selected by Krimigis et.al (3) appears to be an acceptable representation of "quiet time", although it should be noted that numerous periods showing a level of activity below that of the 1972 interval can be seen in the more recent data, particularly during the years 1974-1977. Non-flare, non-quiet time (as defined in this paper) has not been studied previously. However, a study of corotating regions has yielded composition ratios that may be useful for comparison. Gloeckler (2) determined the average composition values of three corotating streams: H/He = 16(+6,-6) and He/(C,O) = 85(+17,-17). These ratios are fairly close to the median non-quiet, non-flare values of H/He = 28(+13,-10) and He/(C,N,O) = 54(+44,-36) of this study.

For the interplanetary medium during all three time components considered, ratios of H/He and He/(C,N,O) assumed values that are similar, though hardly identical, to the results of previous composition studies. The composition ratios measured in this study are significant in that they cover the interplanetary medium over a relatively long period of time. They also characterize three states of the interplanetary medium at solar minimum as displaying substantially different composition features. The distinct distributions seen in H/He and He/(C,N,O) ratios for flare time, quiet time, and non-flare,non-quiet time indicate that very different factors are involved in determining the composition of particle fluxes near the earth for each of these times. These factors may include variations in mechanisms for acceleration and containment of particles as well as the composition of substrates that are the sources of particles seen near the earth.

ACKNOWLEDGMENTS

This work was supported in part by a University of Kansas Undergraduate Research Award and in part by the National Science Foundation through grant #ATM-79-35987 at the Johns Hopkins University Applied Physics Laboratory and via subcontract to the University of Kansas. The author is indebted to T.P. Armstrong and P.R. Briggs for their valuable advice and suggestions for this project.

REFERENCES

(1) Armstrong, T.P., and S.M. Krimigis, "Statistical Study of Solar Protons, Alpha Particles, and Z 3 Nuclei in 1967-68", J. Geophys. Res., 76, 4230, 1971.

(2) Gloeckler, G., D.Hovestadt, F.M. Ipavich, and G.M. Mason, "Distribution Function Representations of Energy Spectra of H, He, C, O and Fe in Corotating Particle Streams", Conference Papers, 16th Int. Cosmic Ray Conference, Kyoto, 1979.

(3) Krimigis, S.M., and T.P. Armstrong, "Measurements of the Relative Abundances of Fe-group, He, and M-nuclei During the October 28,1972 Solar Particle Event", Conference Papers, 13th Int. Cosmic Ray Conference, Denver, 2, 1510, 1973.

Krimigis, S.M., and T.P. Armstrong, and J.W. Kohl, "Measurements of the Quiet-time Low Energy Proton, Alpha, and M-nuclei Component in Cosmic Rays", Conference Papers, 13th Int. Cosmic Ray Conference, Denver, 2, 1656, 1973.

(4) Mason, G.M., L.A. Fisk, D. Hovestadt, and G. Gloeckler, "A Survey of 1 MeV/nucleon Solar Flare Particle Abundances, $1 < Z < 26$, During the 1973-1977 Solar Minimum Period", Ap. J., 239, 1070, 1980.

(5) Armstrong, T.P., and S.M. Krimigis, "Interplanetary Acceleration of Relativistic Electrons Observed with IMP 7", J. Geophys. Res., 81, 677, 1976.

(6) Armstrong, T.P., "Handbook and Reference Manual for Charged Particle Measurement Experiment Data from Explorer 47 and 50", Rep. JHU/APL 76-02, Appl. Phys. Lab., Johns Hopkins University, Laurel, MD., 1976.

(7) Nonnast, J.H., T.P. Armstrong, and J.W. Kohl, "A Study of Solar Flare Soft X-rays and Their Relation to Particle Events Observed with IMP 8", J. Geophys. Res., 87, 4327, 1982.

(8) Briggs, P.R., "Solar and Interplanetary Ions Near Earth", Dissertation, University of Kansas, 1981.

(9) Bertsch, D.L. and S.M. Krimigis, "Interplanetary Acceleration of Relativistic Electrons Observed with IMP 7", J. Geophys. Res., 81, 677, 1976.

(10) Gloeckler, G., "Compositions of Energetic Particle Populations in Interplanetary Space, Rev. Geophys. and Space Phys., 17, 569, 1979.

(11) Mason, G.M. and G. Gloeckler, "Temporal Variations of Nucleonic Abundances in Solar Flare Energetic Particle Events. II. Evidence for Large Scale Shock Acceleration," Submitted to Ap. J., 1984 (preprint).

(12) Cook, W.R., E.C. Stone, and R.E. Vogt, "Elemental Composition of Solar Energetic Nuclei", Ap. J. (Letters), 238, L97, 1980.

(13) Lanzerotti, L.J., and C.G. Maclennan, "Abundance of Solar Cosmic Ray Alpha Particles", J. Geophys. Res., 78, 3935, 1973

FACULTY SPONSOR OF THIS PAPER

Dr. T.P. Armstrong
Department of Physics & Astronomy
The University of Kansas
Lawrence, KS 66045